Presented at the 36th European PV Solar Energy Conference and Exhibition, 9-13 September 2019, Marseille, France

THERMOMECHANICAL EVALUATION OF NEW PV MODULE DESIGNS BY FEM SIMULATIONS

Andreas J. Beinert[1,2], Pascal Romer[1], Martin Heinrich[1], Max Mittag[1], Jarir Aktaa[2] and Dirk Holger Neuhaus[1]
[1]Fraunhofer Institute for Solar Energy Systems ISE, Heidenhofstraße 2, 79110 Freiburg, Germany
[2]Karlsruhe Institute of Technology (KIT), Institute for Applied Materials, Hermann-von-Helmholtz-Platz 1, 76344 Eggenstein-Leopoldshafen, Germany
Corresponding author: Andreas J. Beinert | Phone: +49 (0)761 4588 5630 | E-mail: Andreas.Beinert@ise.fraunhofer.de

ABSTRACT: We present an evaluation of the solar cell and PV module size regarding their impact on thermomechanical stress. The evaluation is based on finite element method (FEM) simulations. Within these simulations, we perform parameter variations of (i) the number of solar cells within a PV module from 60 up to 140 cells, (ii) the cell size from 156.0 mm (M1) up to 161.75 mm (M4) and (iii) the cell format from full cells down to quarter cells. The FEM simulations cover the lamination process and mechanical load of 2400 Pa and 5400 Pa for glass-foil as well as glass-glass modules. The presented results reveal correlations between the solar cell and module size with the stress in solar cells. Our investigations show that the increase of the number of solar cells within a PV module has the largest impact on the stress. However, at a mechanical load of 2400 Pa glass-foil modules with less than 96 solar cells have a negligible failure probability. The advantage of placing the solar cells in the neutral axis of the laminate is proven by the negligible tensile stress values for all variations of glass-glass modules even at 5400 Pa.

Keywords: Finite element modelling, FEM simulations, mechanical load, photovoltaic module, PV module size, solar cell size, stress, thermomechanics, virtual prototyping.

1 INTRODUCTION

In the past, glass-foil PV modules with 60 solar cells have dominated the market. According to the 10th edition of the International Technology Roadmap for Photovoltaic (ITRPV) [1] the market shifts to larger modules, with 60 cell PV modules covering only about 40% in 2029. A similar trend is predicted for the cell format by the ITRPV. In 2029, more than 40% of the PV modules will be made of cut cells, like half or quarter cells. At the same time, the wafer size shifts away from 156 mm edge length to larger wafers and the market share of glass-glass PV modules increases.

In this work, we investigate these trends from a thermomechanical point of view using the finite element method (FEM) to analyze effects of stress related to lamination and mechanical load according to IEC 61215 [2]. We benchmark potential new PV module designs versus a reference design (glass-foil with 60 full-square solar cells of 156.75 mm width).

2 METHOD

We have built a 3D FEM model of a conventional PV module based on two validated models published previously [3–5]. In order to minimize the computational effort, we exploit the twofold axial symmetry of the PV laminate by modelling a quarter laminate. Since the metallization has no significant influence on stress [6], we implement the solar cells as full-square mono-crystalline silicon wafer without metallization. In a previous publication [7], we found that the highest tensile stress occurs at the end of the busbar. Also, the length of the solder joint has no significant influence on the maximum stress occurring from the solder joint [7]. This implies that for the performed variations, the contribution of the solder joint to the total stress is approximately constant. However, the implementation of busbars and ribbons into the FEM model comes with a huge increase in computational resources, therefore, we neglect the ribbons and busbar. The mesh consists of hexahedral elements with 2,700 mesh elements per solar cell and a quadratic serendipity basis function.

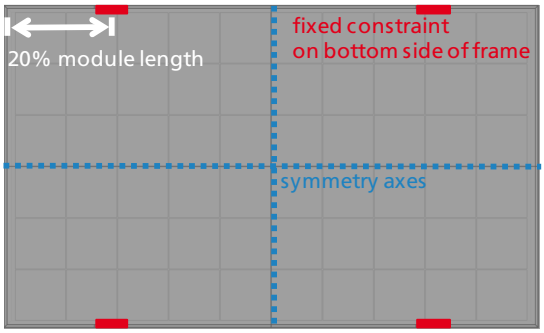

Figure 1: FEM model geometry of the reference module with the symmetry axes depicted (blue lines). The red rectangles show the position of the fixed constraint at 20% of the module length from the edge.

The FEM model covers the lamination process, mechanical load (ML) and thermal cycling (TC). Within this paper the results for lamination and ML are presented, for the TC results we refer to another publication [8]. For the lamination process, the FEM model consists from top to bottom of a glass, encapsulant, solar cells, encapsulant, backsheet/glass. For the mechanical load we add an aluminum frame to the pre-stressed laminate, which is connected to the laminate by a rubber inlay. We simulate the mounting of the framed module on a rack by a fixed constraint on the long side of the module, depicted in Figure 1. The distance to the module edge is 20% of the long side. In a first step, we simulate the lamination process by cooling down from 150 °C to 25 °C. In the second step, we simulate the homogeneous push load of 2400 Pa and 5400 Pa. To consider the residual stress from lamination, we transfer the stress tensor from the lamination to the ML simulation step. We use linear-elastic and temperature dependent material models shown in Table I. For the silicon solar cell we use an anisotropic material model.

Table I: Specifications and material properties of the reference PV module. *: provided by manufacturer, †: measured.

Layer	Material	Dimension	Density [g/cm³]	Young's modulus [GPa]	Poisson's ratio [-]	CTE [10^{-6}K^{-1}]
Front glass	soda-lime glass	3.2 mm	2.5*	70*	0.2*	9*
Encapsulant	EVA	400 µm	0.96 [11]	T-dep.†	0.4 [11]	270 [11]
Solar Cell	Cz-Silicon	156.75 × 156.75 × 0.180 mm³	2.329 [11]	Elasticity matrix [11]		T-dep. [9,10]
Backsheet	TPT	350 µm	2.52 [11]	3.5 [11]	0.29 [11]	50.4 [11]
Frame	aluminium		2.7 [12]	70 [12]	0.33 [12]	23 [12]
Frame-inlay	rubber	8.85 × 1.15 mm²	0.067*	0.0074*	0.3*	769*

The reference within this work is a glass-foil PV module with 60 full format 156.75 mm × 156.75 mm solar cells and a cell gap of 3 mm. The total size is 1.661 m × 0.997 m. From this reference configuration, we vary the number of solar cells, the cell size and the cell format independently from each other with the parameters shown in Table II. Additionally, we simulate each configuration as a glass-foil and glass-glass setup. For the glass-glass setup, the backsheet is replaced by glass, with the front and back glass having a thickness of 2 mm. Please note, that both setups have a frame for a better comparability. The variation of the number of solar cells is composed of an increase of the number of strings (6, 8, 10) per module and an increase of the number of cells per string (10, 12, 14), as illustrated in Figure 2.

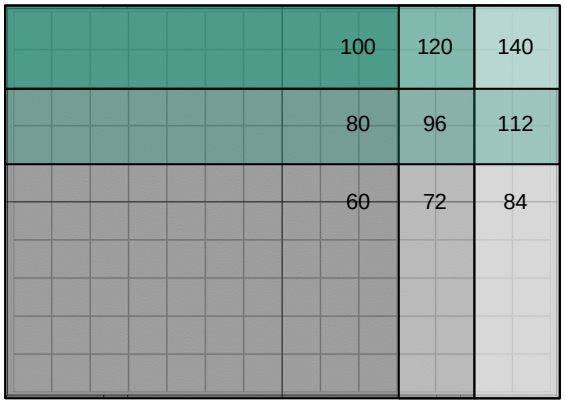

Figure 2: Illustration of the module sizes for the different number of solar cells per module with full 156.75 mm cells. The grey shading indicates the increase in cells per string and the green shading indicates the increase in strings per module.

Table II: PV module design parameters used in the FEM simulations. The reference parameters are underlined.

Glass-foil & glass-glass		
Number of cells	Cell size for 60 cells [mm]	Cell format for 60 cells
60 (6x10)		
72 (6x12)		
84 (6x14)		
80 (8x10)	156.00 (M1)	Full cell
96 (8x12)	156.75 (M2)	Half cell
112 (8x14)	161.75 (M4)	Third cell
100 (10x10)		Quarter cell
120 (10x12)		
140 (10x14)		

We evaluate the FEM simulation results using the principal stresses in the solar cells. During cooling after lamination, the stronger contraction of the front and back layer compress the solar cells. Hence, the dominating stress is compressive (negative stress values). Consequently, we evaluate the minimum stress by using the lowest negative stress value of the third principal stress σ_{III} within the solar cells. As a brittle material, silicon solar cells fail under tensile stress, therefore compressive stress is not crucial for solar cells. However, independently of the direction, high stresses can lead to delamination [13] and interconnector fatigue [14]. When exposed to mechanical load, the dominating stress in the solar cells is tensile. Therefore, we evaluate the maximum of the first principal stress σ_{I} within the solar cells. We convert the obtained maximum first principal stress σ_{I} values from the front and back side of the solar cells into a probability of failure P_{f} using the Weibull distribution [15] considering the size effect [16]:

$$P_{\mathrm{f}} = 1 - \exp\left(- \sum_{\mathrm{i}} A_{\mathrm{eff,i}} \left(\frac{\sigma_{\mathrm{I,max,ref}}}{\sigma_{\mathrm{0,i}}} \right)^{m_{\mathrm{i}}} \right), \qquad (1)$$

with the effective area A_{eff}, the maximum first principal stress of the reference setup $\sigma_{\mathrm{I,max,ref}}$, the Weibull scale factor σ_0 and the Weibull modulus m. The sum is over the values of the front (sunny) and back side, respectively. The effective area A_{eff} can be interpreted as the area of significant stress values and is calculated for the front and back side separately by:

$$A_{\mathrm{eff,i}} = \int \left(\frac{\sigma_{\mathrm{I,i}}(\mathrm{x,y})}{\sigma_{\mathrm{I,max,ref}}} \right)^{m_{\mathrm{i}}} dA_{\mathrm{i}} \,. \qquad (2)$$

The probability of failure P_{f} expresses the likelihood that within one module at least one crack in at least one solar cell occurs. For the Weibull scale factor σ_0 and modulus m we use values from Kaule *et al.* [17] for Al-BSF solar cells, shown in Table III. Due to the cell splitting process, the Weibull distribution is different for cut solar cells. In this work, we consider the laser scribing and cleaving (LSC) process, also given in [17].

Table III: Weibull Parameter used to calculate the probability of failure. Values of Weibull modulus m and characteristic fracture stress σ_θ taken from [17]. Scale factor σ_0 calculated by $\sigma_0 = A_{\mathrm{eff}}^{1/m}\, \sigma_\theta$, using the effective area 9116 mm² given in [17].

Format	Side	Weibull modulus m [-]	Characteristic fracture stress σ_θ [MPa]	Scale factor σ_0 [MPa m²]
full	front	7.8	184	100.8
full	back	6.9	180	91.1
cut	front	8.7	166.4	97
cut	back	17.5	116.1	88.8

We use the thermal expansion stiffness E_α as a measure of the impact the materials have on each other. It is defined as the product of the Young's Modulus E and the coefficient of thermal expansion (CTE) α [18]:

$$E_\alpha = E \cdot \alpha. \quad (3)$$

3 RESULTS

3.1 Lamination

Firstly, we analyze the variation of the number of cells from 60 to 140 cells per module as depicted in Figure 3. The compressive stress for glass-foil modules increases slightly from 84 MPa (60 cells) to 85 MPa (140 cells). The slight dependency of the stress with the cell number after lamination originates from the increase in module size. The module size depends on the number of cells plus the cell gap. Due to the CTE mismatch of the front glass and backsheet, glass-foil modules exhibit a small convex bow after lamination, which adds up to the above mentioned stress originating from the compression of the solar cells by the front and back layer. Moreover, the bow increases with an increasing module size and hence the stress from the bow.

Since the glass-glass module stack is vertically symmetric, it does not exhibit a significant bow after lamination and hence there is no dependency of the number of cells. However, it shows a higher compressive stress of 89 MPa. This higher compressive stress relates to the higher thermal expansion stiffness E_α of glass compared to backsheet. While the glass has a value of 630 kPa/K, the backsheet has a much lower value of 176.4 kPa/K. Additionally, the back-glass is thicker than the backsheet. Consequently, the back glass contracts the solar cell stronger, than the backsheet.

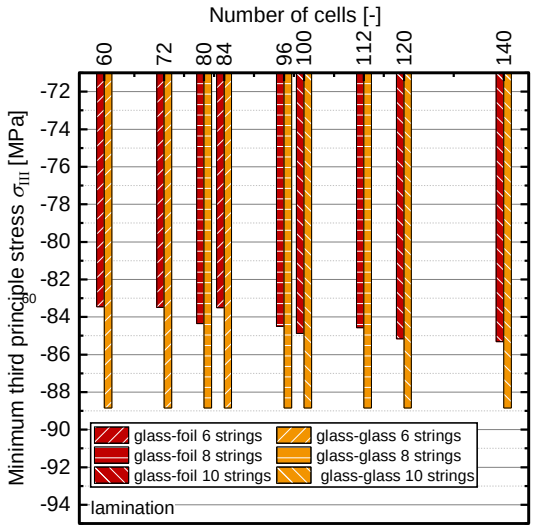

Figure 3: Minimum third principal stress σ_{III} of the cells after lamination for the variation of the number of cells for glass-foil (red) and glass-glass (orange) modules. The shading indicates the number of strings per module.

Secondly, we analyze the variation of cell size shown in Figure 4 (a). The compressive stress after lamination in a glass-foil module slightly increases from 83 MPa (156.0 mm) to 85 MPa (161.75 mm). The slight increase originates on one hand, from the increase of the module size as described above and on the other hand from the larger cell size itself. Since the compressive stress comes from the CTE mismatch of the solar cell with the glass and backsheet, the stress increases from the solar cell edge to its center. Accordingly, an increase in the cell size leads to an increase of the stress in the solar cell center. The latter also applies to glass-glass modules. Consequently, they show a dependency on the cell size, with 89 MPa compressive stress (156.0 mm) to 91 MPa (161.75 mm).

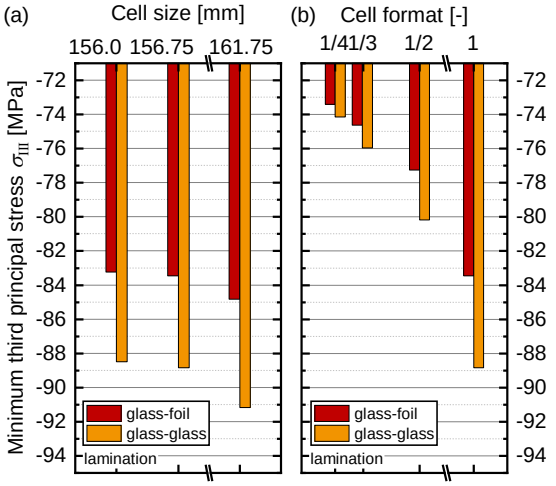

Figure 4: Minimum third principal stress σ_{III} of the solar cells after lamination for the variation of the cell size (a) and cell format (b) for glass-foil (red) and glass-glass (orange) modules.

Thirdly, we analyze the variation of cell format depicted in Figure 4 (b). The compressive stress after lamination in a glass-foil module decreases from 83.5 MPa (full format) to 73.4 MPa (quarter cells). The decrease originates from the decrease of the cell length, as described above. The same applies to glass-glass modules. Consequently, they show a dependency on the cell format, with 89 MPa (full format) to 74 MPa (quarter cells). Again due to the higher thermal expansion stiffness E_α, the dependency is stronger.

3.1 Mechanical Load

2400 Pa push load

Firstly, we analyze the variation of cell number shown in Figure 5. The dependency of the module size is clearly visible for both glass-foil and glass-glass modules. For glass-foil modules the tensile stress increases from 26 MPa (60 cells) to 151 MPa (140 cells), which corresponds to a failure probability of 0.00019% (60 cells) and 98% (140 cells). This shows, that the mounting has to be adapted for modules with a large area, especially with a larger module width. As shown in a previous publication [19], the chosen mounting structure has a huge influence on the stress in solar cells.

Comparing the different number of strings, e.g. the stress for 80 cells (8 strings with 10 cells) and 84 cells (6 strings with 14 cells) shown in Figure 6, shows that adding extra cells to existing strings is more beneficial regarding mechanical stress than adding an extra string. Besides the stronger change of the aspect ratio, the reason is the mounting on the long side of the module. Adding an extra string increases the width of the module without further support, which changes the deflection and

curvature. Further, comparing modules with 96 cells (8 strings with 12 cells) to 100 cells (10 strings with 10 cells), as shown in Figure 6, reveals that a quadratic module shape increases the number of cells with high tensile stress. Both have an almost identical maximum first principal stress σ_I but the more quadratic module with 100 cells has a higher effective area A_{eff} and hence a higher failure probability P_f.

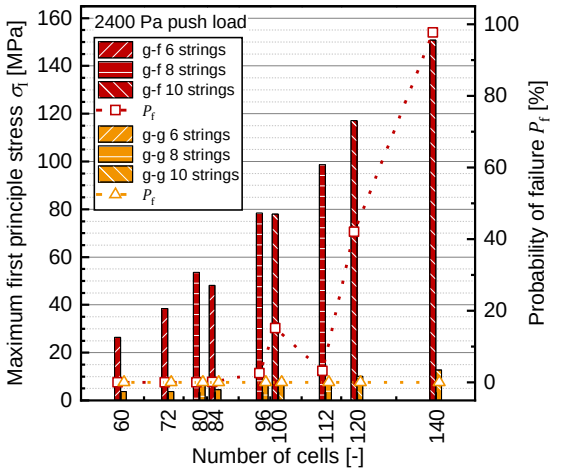

Figure 5: Maximum first principal stress σ_I at 2400 Pa push load (bars, left axis) with the corresponding probability of failure P_f (symbols, right axis) for the variation of the number of solar cells for glass-foil (red) and glass-glass (orange) modules. The shading indicates the number of strings per module.

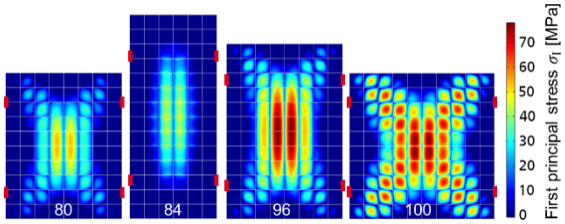

Figure 6: First principal stress on the backside of the solar cells for modules with similar number of cells but different number of strings. The red rectangle indicate the position of the frame mounting.

Due to the symmetric setup of glass-glass modules, the solar cells are in the neutral axis. Accordingly, the tensile stress is very low with 4 MPa (60 cells) and 13 MPa (140 cells). Consequently, the dominating stress is the residual compressive stress from lamination. This results in a negligible probability of failure, even for the modules with a high number of cells.

Secondly, we analyze the variation of cell size depicted in Figure 7 (a) for ML. The tensile stress depends on the solar cell size, since the module size increases with the cell size and hence does the deflection. For the glass-foil setup the tensile stress increases from 26 MPa (156.0 mm) to 32 MPa (161.75 mm). For the glass-glass setup the tensile stress is 4 MPa and does not increase significantly. All stress values correspond to a negligible probability of failure.

Thirdly, we analyze the variation of cell format shown in Figure 7 (b). The tensile stress in glass-foil modules increases from 26 MPa (full cells) to 33 MPa (quarter cells). The increase originates from the increase in module size due to additional cell gaps. Since the cutting process induces additional flaws into the solar cell, the characteristic fracture stress decreases and the Weibull distribution changes. We use the Weibull parameters of half cells from Kaule *et al.* [17], shown in Table III. All stress values correspond to negligible probabilities of failure.

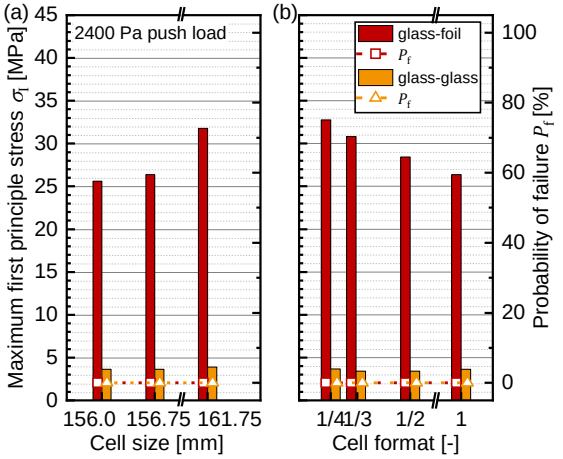

Figure 7: Maximum first principal stress σ_I at 2400 Pa push load (bars, left axis) with the corresponding probability of failure P_f (symbols, right axis) for the variation of the cell size (a) and the cell format (b) for glass-foil (red) and glass-glass (orange) modules.

For glass-glass modules the deflection increases less, hence the increase in tensile stress is lower. Therefore, a second effect appears: The solar cell follows the deformation of the PV module. Consequently, a cut solar cell with a shorter length is less bowed by the PV module's deflection. Thus, the tensile stress slightly reduces with decreasing cell format. For glass-glass modules this effect is slightly stronger than the influence of the PV module size, which leads to a very slight decrease of tensile stress of about 1 MPa.

5400 Pa push load

Qualitatively, the results are in accordance with the 2400 Pa load for all variations. However, the stress values and the according failure probability change dramatically for glass-foil modules. In the following, the results for each variation are discussed.

Firstly, we analyze the variation of the cell number shown in Figure 8. The tensile stress in glass-foil modules ranges from 137 MPa (60 cells) to 434 MPa (140 cells). The corresponding failure probability is 66% for 60 cells, 99% for 72 cells and 100% for modules with more cells. However, since the failure probability is not a measure of the number of cracks, a look at the sum of effective area $A_{eff,module}$ of the front and back side (Figure 9) gives an indication of the severity of cell cracking. Please note, that the effective area is normalized to the maximum first principal stress of the reference $\sigma_{I,max,ref}$ and can be much larger than the PV module area for other variations. For 60 cells it is 0.07 m² and increases to a maximum of 540 m² for 140 cells. Accordingly, much less solar cells are exposed to a critical stress in a 60 cell module compared to module with more cells. Consequently, a lower power loss may be expected.

For glass-glass modules the first principal stress σ_I

also increases to values between 9 MPa (60 cells) to 30 MPa (140 cells). However, these stress values are still considerably low, which results in a negligible failure probability.

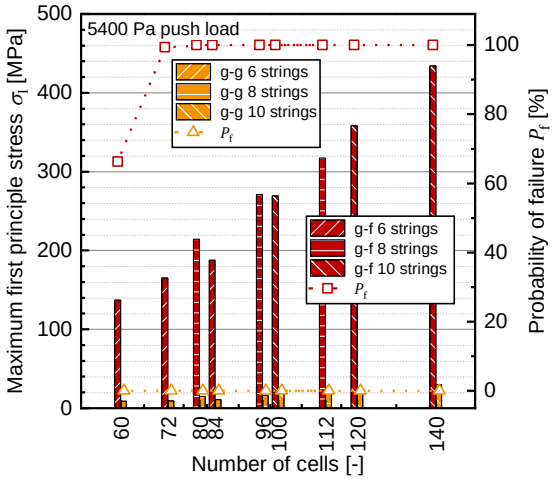

Figure 8: Maximum first principal stress σ_I at 5400 Pa push load (bars, left axis) with the corresponding probability of failure P_f (symbols, right axis) for the variation of the number of solar cells for glass-foil (red) and glass-glass (orange) modules. The shading indicates the number of strings per module.

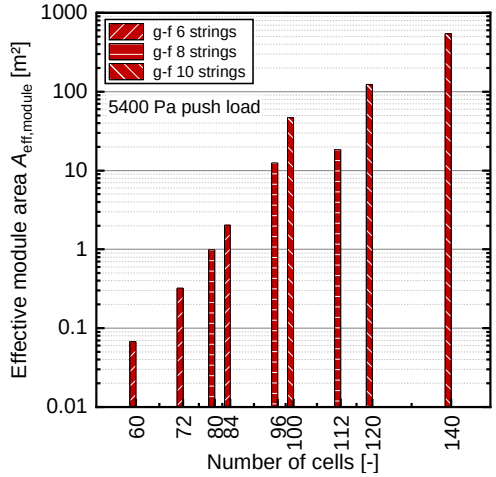

Figure 9: Effective area of the module at 5400 Pa push load for the variation of the number of solar cells for glass-foil modules The shading indicates the number of strings per module. Please note, that the effective area values of the glass-glass modules are not included, because they are negligible.

Secondly, we evaluate the variation of cell size depicted in Figure 10 (a). The tensile stress in glass-foil modules ranges from 135 MPa (156.0 mm) to 152 MPa (161.75 mm). These values correspond to a failure probability of 62% (156.0 mm) and 92% (161.75 mm). Therefore, PV modules with larger cells are more likely to get cells cracks. For the glass-glass setup the tensile stress is 9 MPa and does not increase significantly. All stress values correspond to negligible failure probabilies.

Thirdly, we evaluate the variation of the cell format, depicted in Figure 10 (b). Here, the tensile stress in glass-foil modules increases from 137 MPa (full cells) to 157 MPa (quarter cells). Although, the tensile stress values for cut cells are just a little higher, the failure probability increases from 66% for full cells to 100% for all cut cells, due to the weaker cell edge. Please note, that this holds only for solar cells split with the LSC process. Solar cells split with the thermal laser separation (TLS) process have a higher fracture strength [17] and accordingly the failure probability would be lower.

Due to the higher deflection, the effect that smaller cells are less bent by the module (observed in glass-glass modules at 2400 Pa), is no longer visible. The tensile stress is 9 MPa and slightly decreases with decreasing cell format. Again, all values correspond to negligible failure probabilities.

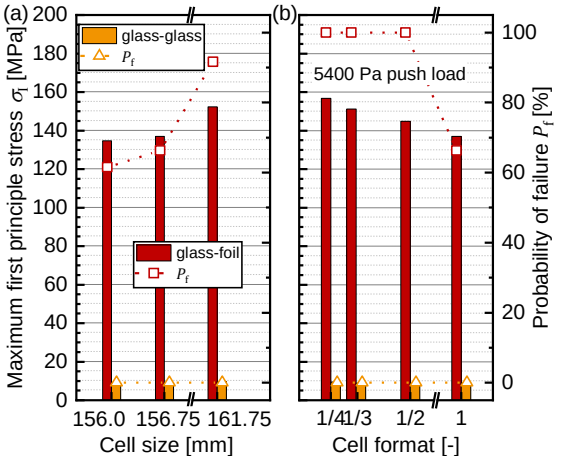

Figure 10: Maximum first principal stress σ_I at 5400 Pa push load (bars, left axis) with the corresponding probability of failure P_f (symbols, right axis) for the variation of the cell size (a) and cell format (b) for glass-foil (red) and glass-glass (orange) modules.

4 CONCLUSIONS

We present a thorough study of solar cell and PV module dimensions and their impact on the thermomechanical stress in PV modules. We perform FEM simulations that cover the lamination process and mechanical load of 2400 Pa and 5400 Pa for glass-foil and glass-glass modules.

The tensile stress from mechanical load of 2400 Pa increases for an increased number of cells per module, as well as for an increase in cell size and when going from full format cells to cut cells. However, all investigated variations have non-critical stress values, except for glass-foil modules with 100 solar cells and more. To prevent cell cracking during mechanical loads, the mounting has to be adapted for modules with a larger and unconventional width. For glass-glass modules the stress and the corresponding probability of failure are negligible for all investigated variations. They benefit from the position of the solar cells in the neutral axis, which reduces the stress to negligible values. This becomes even more evident at 5400 Pa load. While for glass-foil modules, the tensile stress increases significantly and leads to cell cracking of different extent for all variations, glass-glass modules with aluminum frames still have negligible failure probabilities.

Lamination induces compressive stress in the solar cells, which is not responsible for cell cracks but can

induce delamination and ribbon fatigue. The number of solar cells has only a minor impact on the compressive stress. Changing from full format cells to cut cells decreases the compressive stress as well as increasing the solar cell size does.

Finally, it can be concluded, that increasing the number of cells per string induces less stress than increasing the number of strings per module. The change from 156.00 mm to 161.75 mm solar cells influences the stress of cells in the PV module as well as decreasing the cell format. However, both have a smaller impact than increasing the cell number for example from 60 to 72 cells when considering mechanical loads. The simulation results show that glass-glass modules benefit from the solar cells being in the neutral axis.

5 ACKNOWLEDMENT

This work was supported by a PhD scholarship of the Cusanuswerk, Bonn, Germany.

6 REFERENCES

[1] ITRPV International Technology Roadmap for Photovoltaic (ITRPV): 2018 Results, 10th edition, 10th ed. (2019).

[2] IEC IEC 61215-2:2016, Terrestrial photovoltaic (PV) modules – Design qualification and type approval – Part 2: Test procedures (2016).

[3] A.J. Beinert, R. Leidl, P. Sommeling, U. Eitner, J. Aktaa, Proceedings of the 33rd European Photovoltaic Solar Energy Conference and Exhibition (EUPVSEC) (2017), 42–47.

[4] A.J. Beinert, A. Büchler, P. Romer, V. Haueisen, L.C. Rendler, M.C. Schubert, M. Heinrich, J. Aktaa, U. Eitner, Sol Energ Mat Sol C 193 (2019), 351–360.

[5] A.J. Beinert, A. Büchler, P. Romer, M. Heinrich, M.C. Schubert, J. Aktaa, U. Eitner, Proceedings of the 7th World Conference on Photovoltaic Energy Conversion (WCPEC-7) (2018), 3613–3617.

[6] S. Dietrich Numerische Untersuchungen zur mechanischen Zuverlässigkeit verkapselter Siliziumsolarzellen. Dissertation, Fraunhofer-Inst. für Werkstoffmechanik IWM, Halle (Saale) (2014).

[7] L.C. Rendler, P. Romer, A.J. Beinert, J. Walter, S. Stecklum, A. Kraft, U. Eitner, S. Wiese, Sol Energ Mat Sol C 196 (2019), 167–177.

[8] A.J. Beinert, P. Romer, M. Heinrich, M. Mittag, J. Aktaa, H. Neuhaus, IEEE J. Photovoltaics (2019).

[9] R.B. Roberts, Journal of Physics D: Applied Physics 14 (1981), L163.

[10] R.B. Roberts, Journal of Physics D: Applied Physics 15 (1982), L119.

[11] U. Eitner, S. Kajari-Schroeder, M. Köntges, H. Altenbach, in: H. Altenbach, V.A. Eremeyev (Eds.), Shell-like Structures: Non-classical Theories and Applications, Springer, Berlin/Heidelberg, 2011.

[12] W.M. Haynes (Ed.) CRC handbook of chemistry and physics, CRC Press, 2014.

[13] M. Knausz, G. Oreski, M. Schmidt, P. Guttmann, K. Berger, Y. Voronko, G. Eder, T. Koch, G. Pinter, Polymer Testing 44 (2015), 160–167.

[14] S. Wiese, R. Meier, F. Kraemer, Proceedings of the 11th IEEE International Conference on Thermal, Mechanical and Multi-Physics Simulation and Experiments in Microelectronics and Microsystems (EuroSimE) (2010), 1–5.

[15] W. Weibull A Statistical Theory of the Strength of Materials, Generalstabens Litografiska Anstalts Förlag, Stockholm (1939).

[16] D. Munz, T. Fett Ceramics: Mechanical properties, failure behaviour, materials selection, 1st ed., Springer, Berlin | Heidelberg (2001).

[17] F. Kaule, M. Pander, M. Turek, M. Grimm, E. Hofmueller, S. Schönfelder, AIP Conference Proceedings 1999 (2018), pp. 020013-1–020013-9.

[18] W. Carroll, E. Cuddihy, M. Salama, Proceedings of the 12th IEEE photovoltaic specialists conference (1976), 332–339.

[19] A.J. Beinert, M. Ebert, U. Eitner, J. Aktaa, Proceedings of the 32nd European Photovoltaic Solar Energy Conference and Exhibition (EUPVSEC) (2016), 1833–1836.